A crystal-chemical investigation of clinozoisite synthesized along the join Ca₂Al₃Si₃O₁₂(OH)-Ca₂Al₂CrSi₃O₁₂(OH)

MARIKO NAGASHIMA,[1,2,*] CHARLES A. GEIGER,[1] AND MASAHIDE AKASAKA[3]

[1]Institut für Geowissenschaften, Abteilung Mineralogie, Christian-Albrechts-Universität zu Kiel, D-24098 Kiel, Germany
[2]Mineralogical Crystallography, Institute of Geological Sciences, University of Bern, Freiestrasse 3, CH-3012 Bern, Switzerland
[3]Department of Geoscience, Faculty of Science and Engineering, Shimane University, Matsue 690-8504, Japan

ABSTRACT

Cr^{3+}-bearing clinozoisite along the join $Ca_2Al_3Si_3O_{12}(OH)$-$Ca_2Al_2Cr^{3+}Si_3O_{12}(OH)$ was synthesized using cold-seal pressure vessels at $P_{H_2O} = 0.35$ to 0.40 GPa and $T = 500$ °C and a piston-cylinder apparatus at $P_{H_2O} = 0.8$ to 1.5 GPa and $T = 500$ to 800 °C. Gel-starting materials of $Ca_2Al_{3-q}Cr_q^{3+}Si_3O_{12.5}$ composition with $q = 1.00, 0.75, 0.50$, and 0.25 were employed to maximize the yields of clinozoisite. Mass fractions of clinozoisite in the experimental products with $q = 0.50, 0.75$, and 1 were about 70 to 90% along with lesser amounts of eskolaite, garnet, and quartz. Clinozoisite crystallized from the gel with $q = 0.25$ was associated only with zoisite. The crystal structures of clinozoisite in four runs, containing 0.28, 0.49, 0.50, and 0.62 Cr apfu were refined using X-ray powder diffraction data and the Rietveld method. The amount of Cr^{3+} at the octahedral M3 and M1 sites ranged from 0.37(1)–0.16(1) to 0.25(1)–0.12(1) apfu, respectively. Corresponding $K_D = (Cr^{3+}/Al)^{M1}/(Cr^{3+}/Al)^{M3}$ values range between 0.57 and 0.73. The M2 site contained only Al. The K_D values, and published results for intracrystalline partitioning in epidote and piemontite, show that the preference of Cr^{3+} for M1 is stronger than that of Fe^{3+} and Mn^{3+} in spite of the fact that most Cr^{3+} is partitioned into M3. Unit-cell parameters of clinozoisite increase with increasing Cr^{3+}. Variations in macroscopic unit-cell parameters can be related to variations in the local M3-O*i* and M1-O*i* distances.

Keywords: Clinozoisite, zoisite, chromium, synthesis, crystal chemistry, Rietveld refinement

INTRODUCTION

The epidote-amphibole facies is an integral part of the metamorphic facies concept (Eskola 1920), and epidote-group minerals in the system $Ca_2Al_3Si_3O_{12}(OH)$-$Ca_2Al_2Fe^{3+}Si_3O_{12}(OH)$-$Ca_2Al_2Mn^{3+}Si_3O_{12}(OH)$ often occur in low- to medium-grade metamorphic mafic assemblages, hydrothermally altered rocks, and low-temperature veins and joint fillings (Deer et al. 1986). Cr^{3+}-containing clinozoisite and epidote, $Ca_2(Al,Cr^{3+})_3Si_3O_{12}(OH)$, are less common, but they have been reported from several localities worldwide (e.g., Eskola 1933; Grapes 1981; Ashley and Martyn 1987; Treloar 1987; Sánchez-Vizcaíno et al. 1995; Devaraju et al. 1999; Nagashima et al. 2006). The term "tawmawite" was proposed years ago for Cr^{3+}-analog of epidote (Bleeck 1907). However, its composition does not show epidote-group stoichiometry, and no epidote-group mineral with Cr > 0.5 atoms per formula unit (apfu) at M3 has been confirmed. Thus, it is not considered as a valid species name (Armbruster et al. 2006).

Several synthesis and/or phase-equilibrium studies on $Ca_2Al_3Si_3O_{12}(OH)$-$Ca_2Fe_3^{3+}Si_3O_{12}(OH)$, $Ca_2Al_3Si_3O_{12}(OH)$-$Ca_2Mn_3^{3+}Si_3O_{12}(OH)$, and $Ca_2Al_3Si_3O_{12}(OH)$-$Ca_2Fe_3^{3+}Si_3O_{12}(OH)$-$Ca_2Mn_3^{3+}Si_3O_{12}(OH)$ epidote-group solid solutions have been carried out to investigate their stability relations and/or crystal-chemical properties (Coes 1955; Fyfe 1960; Winkler and Nitsch 1963; Strens 1964; Holdaway 1966, 1972; Liou 1973; Anastasiou

and Langer 1977; Keskinen and Liou 1979, 1987; Schiffman and Liou 1983; Giuli et al. 1999; Akasaka et al. 2000; Langer et al. 2002; Brunsmann et al. 2002; Nagashima and Akasaka 2004; Nagashima 2006). However, to the best of our knowledge, there have been no systematic investigations of synthetic Cr-bearing epidote-group minerals. To understand their crystal-chemical properties and the partitioning behavior of Cr among the three crystallographically distinct octahedral sites, M1, M2, and M3, Nagashima et al. (2007) investigated three natural Cr^{3+}-bearing epidote crystals from Iratsu, central Shikoku, Japan. Using X-ray single-crystal diffraction, ^{57}Fe Mössbauer spectroscopy and optical spectroscopy, they determined that Fe^{3+} much prefers M3 over M1 and M2, whereas Cr^{3+} showed less preference as indicated by $K_D = (Cr^{3+}/Al)^{M1}/(Cr^{3+}/Al)^{M3} = 0.35–0.41$. However, because the Iratsu epidote also contained about 0.5 Fe^{3+} apfu and other cations such as Sr (0.08–0.15 apfu), it was difficult to determine quantitatively the effect of Al-Cr^{3+} exchange on crystal-structure properties. Armbruster et al. (2006) cited preliminary X-ray results for natural Cr^{3+}-containing clinozoisite that indicated a slight preference of Cr^{3+} for M3 relative to M1.

In the present study, strictly binary $Ca_2Al_3Si_3O_{12}(OH)$-$Ca_2Al_2Cr^{3+}Si_3O_{12}(OH)$ solid solutions were synthesized to determine the distribution behavior of Cr^{3+} and its effect on the clinozoisite crystal structure. We discuss herein (1) results of synthesis experiments on Cr^{3+}-bearing clinozoisite; (2) X-ray powder structural refinements on four Cr^{3+}-bearing clinozoisite

* E-mail: mariko.nagashima@krist.unibe.ch

samples of different composition; and (3) the crystal chemistry of clinozoisite, especially with regard to Cr^{3+} partitioning behavior.

EXPERIMENTAL METHODS

Synthesis experiments

In preliminary hydrothermal synthesis experiments using conventional oxide mixtures, cristobalite, CaO, α-Al_2O_3, and Cr_2O_3, as starting materials, the experimental products contained only small amounts of clinozoisite but considerable amounts of quartz, anorthite, and chromatite ($CaCr^{6+}O_4$), with a small amount of eskolaite (Cr_2O_3). Therefore, it was decided to switch to gel-starting materials to improve the yields of Cr^{3+}-bearing clinozoisite. Gels were prepared following the method of Hamilton and Henderson (1968). Each reagent-grade chemical was treated as follows: $CaCO_3$ and Cr_2O_3 were dried at 110 °C overnight and γ-Al_2O_3 was heated at 1100 °C for 3 h. Appropriate amounts of $CaCO_3$, Al_2O_3, and Cr_2O_3 were then weighed out and mixed to produce four different bulk compositions defined by $Ca_2Al_{3-q}Cr_q^{3+}Si_3O_{12.5}$, where $q = 1.00$, 0.75, 0.50, and 0.25. The oxides were then dissolved in nitric acid and mixed into a solution of TEOS, $(C_2H_5O)_4Si$. Ammonium hydroxide was added for the precipitation of silica. The gel was dried at room temperature and then heated at 800 °C in air for 3 h.

A series of low-pressure syntheses was undertaken in conventional cold-seal pressure vessels in horizontal geometry, using water as a pressure medium. The experimental conditions were $P_{H_2O} = 0.35$–0.40 GPa and $T = 500$ °C for 21 days. Temperatures were measured using chromel-alumel thermocouples. Experimental pressures and temperatures are precise to ±0.0025 GPa and ±4 °C, respectively. The gel-starting materials, ca. 0.3 g, were sealed in Au capsules of 5 mm diameter containing distilled water in excess of that required for crystallization of clinozoisite.

Syntheses were also performed at higher pressures at $P_{fluid} = 0.8$–1.5 GPa and $T = 500$–800 °C in a piston-cylinder apparatus using a NaCl-based cell assembly (Cemic et al. 1990). Temperatures were measured and controlled by means of sheathed Ni/NiCr thermocouples. Experimental pressures and temperatures are precise to about ±0.1–0.2 GPa and ±10 °C, respectively. The starting materials, ca. 0.1 g, were sealed in Ag capsules (5 mm in external diameter and 1 cm long) containing an excess amount of distilled water. Run durations were from 21 to 71 h. The mineral assemblages indicate that Cr stabilized as trivalent under the experimental conditions in this study.

Phase identification

The experimental synthesis products were characterized using an automated SIEMENS D-5000 X-ray powder diffractometer with Cu$K\alpha$ radiation at the University of Kiel. Step-scan data were collected between 5 and 60 °2θ using a step interval of 0.04° and a step counting time of 2 s.

Chemical analysis

The compositions of the synthetic phases were determined using a JEOL JXA-8900 electron probe microanalyzer operated at 15 kV, with a beam current of 20 nA and beam diameter of 1 μm. The standards used were wollastonite for Ca and Si, corundum for Al, and chromite for Cr. The modified ZAF (PRZ) method with $\phi(\rho Z)$ integration for the atomic number correction (Packwood and Brown 1981; Bastin et al. 1984, 1986) was used for data correction.

X-ray powder diffraction data collection and Rietveld analysis

The synthesis products were ground using an agate mortar until the grain size was <2 μm. This is necessary to obtain good X-ray powder diffraction data needed for Rietveld refinement (Bish and Reynolds 1989; Post and Bish 1989). The samples were mounted on a silicon single-crystal plate that yields a low and flat diffraction background. Diffractograms were recorded using a PANalytical X'Pert Pro MPD θ/θ X-ray diffractometer equipped with a RTMS detector at the University of Bern with Cu$K\alpha$ radiation generated at 40 kV and 40 mA. Soller slits (0.04 rad), an anti-scattering slit (0.25°), and a divergence slit (0.125°) were mounted in the incident beam pathway. The diffracted beam pathway included an antiscatter slit (0.125°), soller slits (0.04 rad) and a Ni filter. Diffractograms were collected using 70–80 s step[-1] (step-size 0.008 °2θ) over the angular range 5 to 130 °2θ.

The clinozoisite crystal structures were refined using the RIETAN-FP program of Izumi and Momma (2007). The observed diffractograms, obtained under the measuring condition of 0.008 °2θ step[-1], were interpolated to a value of 0.02 °2θ

step[-1] by PANalytical X'Pert HighScore, because the recommended step-interval should be one-fifth to one-half of the minimum full-width at half maximum for resolved peaks in the pattern (Hill and Madsen 1986). The minimum FWHM in this study ranged from 0.08 to 0.13°. Positions for the atoms in clinozoisite (Dollase 1968), epidote (Dollase 1971), eskolaite (Newnham and De Haan 1962), and grossular (Geiger and Armbruster 1997) were taken from the cited works and used as starting parameters in the Rietveld refinement. Since the both neutral and ionized X-ray scattering factors for constituent elements gave essentially the same results, the former were employed in the refinement. Isotropic displacement parameters for the atoms in clinozoisite were fixed to the values obtained by Dollase (1971). Peak profiles were defined using the "Split Pearson VII function" of Toraya (1990) or a modified split pseudo-Voigt function (Izumi and Ikeda 2000) combined with profile relaxation. An asymmetric parameter is built into this profile function and further details are given in Izumi and Ikeda (2000). Non-linear least-squares calculation using the Marquardt method was followed by the conjugate-direction method to check convergence at local minima (Izumi 1993). Preferred orientation for (010) in clinozoisite was corrected using the March-Dollase function (Dollase 1986).

RESULTS

Description of synthesis products

The synthesis conditions and the resulting products for the different experiments are listed in Table 1. Upon opening all capsules, moisture was observed, thus indicating water-saturated conditions during the experiment. The phases obtained from the oxide-starting material with $q = 1.00$ at 0.40 GPa and 500 °C (experiment G1) and 0.35 GPa and 500 °C (G2) consisted of Cr-bearing grossular, Cr^{3+}-bearing clinozoisite, eskolaite, anorthite, and quartz, with Cr-bearing grossular as the predominant phase and a minor amount of clinozoisite. In contrast, larger amounts of clinozoisite, associated with minor eskolaite + Cr-bearing grossular ± quartz, crystallized from the gel-starting material for $q = 1.00$ at 0.8–1.5 GPa and 600–800 °C (Fig. 1a). The products

TABLE 1. Experimental synthesis results

| Exp. no. | q^* | Run condition | | | Mineral assemblege‡ |
		P (GPa)	T (°C)	Duration†	
Experiments at 0.35–0.40 GPa					
G1	1.00	0.40	500	21 d	Grs>Cz>An, Qz, Esk
G2	1.00	0.35	500	21 d	Grs>>Cz>An, Qz, Esk
Experiments at 0.8–1.5 GPa					
G3	1.00	1.5	800	22 h	Cz>>Grs, Esk
G4	1.00	1.5	700	22 h	Cz>>Grs, Esk
G5	1.00	1.5	700	24 h	Cz>>Grs, Qz, Esk
G7	1.00	1.5	700	23 h	Cz>>Grs, Esk
G8	1.00	1.5	600	22 h	Cz>>Qz>Grs, Esk
G9	1.00	1.2	700	21 h	Cz>>Grs, Esk
G12	1.00	0.8	700	21 h	Cz>>Grs, Esk
G17	1.00	1.2	600	71 h	Cz>Grs>Qz, Esk
G31	1.00	1.2	700	23 h	Cz>>Grs>Qz, Esk
G26	0.75	1.2	600	24 h	Cz>>Grs>Esk
G27	0.75	1.2	700	21 h	Cz>>Grs, Esk
G28	0.75	1.2	600	24 h	Cz>>Esk
G10	0.50	1.5	700	23 h	Cz>>Grs>Esk
G11	0.50	1.5	600	23 h	Cz>>Grs, Qz
G13	0.50	1.2	700	22 h	Cz>>Grs>Qz, Esk
G15	0.50	1.5	500	21 h	Cz>Qz>Grs>Esk
G16	0.50	1.2	600	23 h	Cz>Qz>Grs>Esk
G18	0.50	1.2	600	47 h	Cz>>Qz,Grs>Esk
G20	0.50	1.2	600	24 h	Cz>>Qz>Grs
G22	0.50	1.2	700	23 h	Cz>>Grs
G24	0.50	1.2	600	23 h	Cz>>Grs, Qz
G30	0.50	1.2	700	24 h	Cz>>Grs, Qz>Esk
G32	0.25	1.2	700	24 h	Cz>Zo
G33	0.25	1.2	600	22 h	Cz>Zo

* $q = Cr^{3+}$ in $Ca_2Al_{3-q}Cr_q^{3+}Si_3O_{12.5}$ starting material.
† d = days; h = hours.
‡ An = anorthite; Cz = Cr^{3+}-bearing clinozoisite; Esk = eskolaite; Grs = Cr-bearing grossular; Qz = quartz; Zo = zoisite.

from the gel-starting material with $q = 1.00$ (i.e., G3, G4, G5, G7, G8, G9, G12, G17, and G31 in Table 1) were green in color, whereas those crystallized from the gel-starting material with q = 0.75 (i.e., G26, G27, and G28) at 1.2 GPa and 600–700 °C were pale green. The products from experiments G26 and G27 consisted of Cr^{3+}-bearing clinozoisite, eskolaite, and Cr-bearing grossular, and that of G28 of clinozoisite and eskolaite (Fig. 1b). The phases crystallized from the starting material with q = 0.50 at 1.2–1.5 GPa and 500–700 °C are also pale green in color and consist of clinozoisite + Cr-bearing grossular ± quartz ± eskolaite. The amount of eskolaite is positively correlated with the bulk Cr^{3+} content in the starting gel, but the amount of Cr-bearing grossular was not. The products from the q = 0.25 starting material consisted only of Cr^{3+}-bearing clinozoisite and

zoisite (G32 and G33) (Fig. 1c).

Clinozoisite that crystallized from the gel-starting materials with q = 1.00, 0.75, and 0.50 consisted of fine-grained euhedral prismatic crystals about 1 to 2 μm in length and less than 0.5 μm in width (Fig. 2a). In comparison, Cr^{3+}-bearing clinozoisite crystallized from the gel-starting material with q = 0.25 were slightly larger, being about 5 μm in length with a maximum width of 3 μm (Fig. 2b).

Chemical composition of the experimental products

The average chemical compositions of the clinozoisite from experiments G27, G28, and G22, and clinozoisite and zoisite from G32 and G33, are listed in Table 2. Those for the other synthesis experiments were too fine grained to be analyzed using standard electron microprobe techniques. In terms of the determined compositions, the oxidation state of Cr was assumed to be trivalent, which is consistent with the observed mineral assemblages.

The Cr contents of clinozoisite from the G27 and G28 syntheses (q = 0.75) are 0.50 apfu and identical within their error limits (Table 2). Their compositions represent about two thirds of the bulk Cr content in the starting material. The Cr contents of clinozoisite in G22 from the starting material with q = 0.50 is 0.28 Cr apfu. The Cr content of clinozoisite from the q = 0.25 starting material is 0.24 apfu for experiments G32 and G33. Both reflect the bulk Al:Cr^{3+} ratio of the starting material, i.e., Al:Cr^{3+} = 2.75:0.25. The coexisting zoisite in G32 and G33 is poorer in Cr, having 0.15 and 0.13 Cr apfu, respectively. The Cr^{3+} contents in clinozoisite and zoisite range between 0.21 to 0.32 and 0.07 to 0.19 apfu, respectively. Although eskolaite was not identified by X-ray powder diffraction analysis in G32 and G33, trace amounts were observed in the microprobe measurements.

Rietveld refinements

The crystal structures of Cr^{3+}-bearing clinozoisite from G22, G27, G28, G32, and G33 (Table 2) were refined using the Rietveld method (Rietveld 1967). Associated phases such as eskolaite and/or Cr-bearing grossular were also included in the refinements for G22, G27, and G28. A summary of the results is given in Table 3. The resulting goodness-of-fit values ($S = R_{wp}/$
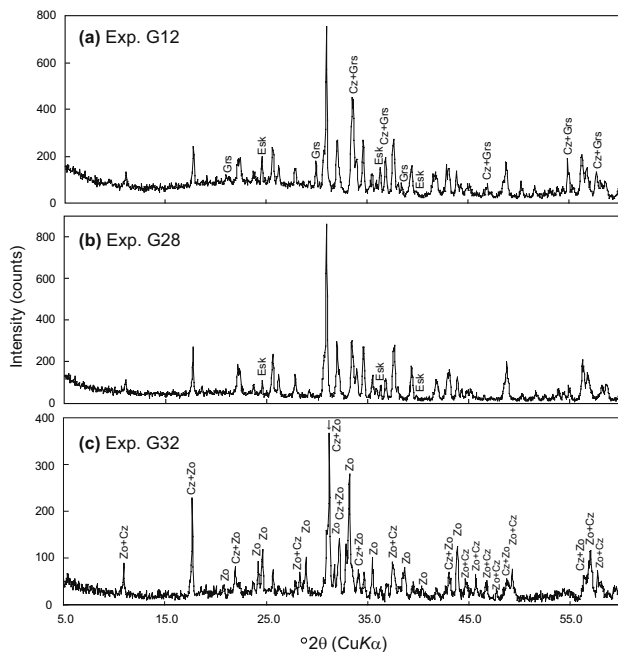

FIGURE 1. X-ray powder diffraction patterns of experimental products; Cz = Cr^{3+}-bearing clinozoisite, Esk = eskolaite, and Grs = Cr-bearing grossular. Peaks without labels belong to Cr^{3+}-bearing clinozoisite. Synthesis conditions are given in Table 1.
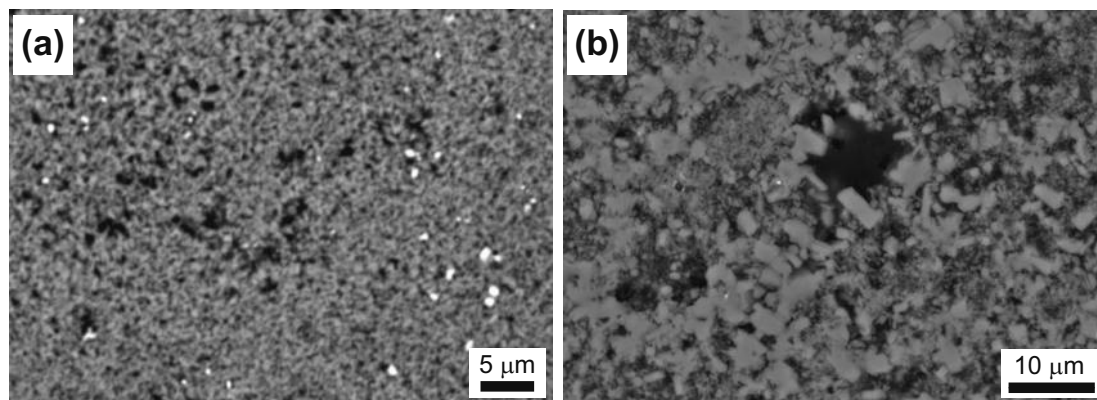

FIGURE 2. SEM images of experimental products. (**a**) G9 from q = 1.00 starting material showing prismatic Cr-bearing clinozoisite and eskolaite crystals (white spots) and (**b**) G33 from q = 0.25 starting material showing euhedral zoisite and clinozoisite crystals and trace amounts of eskolaite (very small white spots).

TABLE 2. Average chemical compositions of Cr^{3+}-bearing clinozoisite and zoisite

q^*	0.75				0.50		0.25							
P (GPa)	1.2		1.2		1.2		1.2				1.2			
T (°C)	700		600		700		700				600			
Exp. no.	G27		G28		G22		G32				G33			
Phase†	Cz		Cz		Cz		Cz		Zo		Cz		Zo	
	n = 10		n = 8		n = 8		n = 9		n = 11		n = 8		n = 13	
	avg.	s.d.	avg.	s.d.	avg.	s.d.	avg.	s.d.	avg.	s.d.	avg.	s.d.	avg.	s.d.
SiO_2	38.29	0.35	37.98	0.52	39.05	0.52	39.06	0.40	39.12	0.34	38.92	0.29	39.28	0.37
Al_2O_3	27.10	0.62	27.00	1.63	29.48	0.91	30.41	0.46	31.35	0.50	29.96	0.41	31.69	0.69
Cr_2O_3	8.00	0.50	7.88	1.65	4.53	0.24	4.00	0.36	2.50	0.56	3.96	0.67	2.08	0.68
CaO	23.78	0.24	23.69	0.22	24.12	0.14	24.27	0.22	24.40	0.16	24.05	0.29	24.48	0.29
Total	97.17		96.55		97.18		97.74		97.37		96.89		97.53	
Cations per 12.5 O atoms														
Si	3.00	0.01	3.00	0.03	3.02	0.05	3.00	0.01	3.00	0.01	3.02	0.02	3.01	0.01
Al	2.50	0.03	2.51	0.14	2.69	0.07	2.75	0.02	2.84	0.04	2.74	0.04	2.86	0.04
Cr	0.50	0.03	0.49	0.11	0.28	0.01	0.24	0.02	0.15	0.03	0.24	0.04	0.13	0.04
Ca	2.00	0.02	2.00	0.02	2.00	0.01	2.00	0.01	2.01	0.02	2.00	0.02	2.01	0.01
Total	8.00		8.00		7.99		7.99		8.00		8.00		8.01	

* $q = Cr^{3+}$ in $Ca_2Al_{3-q}Cr_q^{3+}Si_3O_{12.5}$ starting material.
† Abbreviations as in Table 1.

R_e) are between 1.02–1.12, and the Durbin-Watson d statistic is 0.97–1.21. A refinement of the experimental products from the $q = 0.75$ starting material at 1.2 GPa and 700 °C (G27) is shown in Figure 3 as an example. Figure 4 shows the polyhedral crystal structure of clinozoisite based on a refinement from experiment G9. The synthetic products from G32 and G33 consisted of clinozoisite and zoisite and, thus, their diffractograms were refined with both phases. However, their S and Durbin-Watson d statistics were >1.8 and <0.4, respectively, even though the analyses showed (1) mass fractions of clinozoisite and zoisite of about 0.7 and 0.3, respectively; (2) site occupancies of Cr at M1 and M3 of 0.08 and 0.16, respectively, which follow the regression line of G22, G27, and G28 (discussed below); and (3) reasonable structural parameters. The reason for the large statistical errors associated with the refinements of G32 and G33 is not clear. Perhaps additional unidentified phase(s) were present, resulting in overlapped clinozoisite and zoisite. Thus, these results were not used for further analysis.

On the basis of the EMPA data, the Ca occupancies at the A1 and A2 sites and the Si occupancy at the T sites were set at 1.0. Preliminary refinements of the Cr occupancies at the M1, M2, and M3 sites resulted in less than 5% or negative Cr occupancies at M2. Thus, its occupancy was fixed to 1.0 Al atom. For G27, G28, and G22, the occupancies for Al and Cr^{3+} at M1 (Al_{M1} and Cr_{M1}) and M3 (Al_{M3} and Cr_{M3}) were refined using the following constraints: $Cr_{M1} = 1.0 - Al_{M1}$, $Cr_{M3} = Cr_{total} - Cr_{M1}$, and $Al_{M3} = 1.0 - Cr_{M3}$, where Cr_{total} is the total number of Cr atoms determined by microprobe analysis. The composition of clinozoisite from experiment G9 was not analyzed because of its very fine crystal size. Its Cr_{total} apfu (y) was estimated from Cr^{3+} apfu (x) values derived from the unconstrained Cr occupancies at M1 and M3 by applying the relationship $y = 1.364x - 0.004$. This equation was established from EMPA analyses and Rietveld analyses using results on clinozoisite from G27, G28, and G22. The calculated Cr_{total} for clinozoisite from G9 is 0.62 apfu, which was used to constrain the Cr^{3+} content in the refinement.

Refined atomic positions and cation occupancies for the octahedral sites are given in Tables 4 and 5, respectively. Selected interatomic distances and bond angles are listed in Tables 6 and 7, respectively. It is known that by increasing the counting time

TABLE 3. Data collection* and details of structure refinement

q†	1.00	0.75		0.50
Synthesis P (GPa)	1.2	1.2	1.2	1.2
T (°C)	700	700	600	700
Exp. no.	G9	G27	G28	G22
Cr^{3+} content (apfu)	0.62‡	0.50§	0.49§	0.28§
Max. intensity (counts)	5005	5905	5859	5202
Clinozoisite ($P2_1/m$)				
a (Å)	8.8889(3)	8.8859(3)	8.8841(3)	8.8806(3)
b (Å)	5.6058(1)	5.6006(1)	5.6022(1)	5.5973(1)
c (Å)	10.1513(3)	10.1500(3)	10.1480(3)	10.1465(3)
β (°)	115.284(2)	115.322(2)	115.320(2)	115.312(2)
V (Å³)	457.4(5)	456.6(4)	456.5(4)	455.9(5)
Z	2	2	2	2
R_B (%)‖	4.11	4.01	2.89	3.20
R_F (%)‖	3.06	2.38	1.38	1.53
Eskolaite ($R\bar{3}c$)				
a (Å)	4.9607(5)	4.9620(7)	4.9609(2)	
c (Å)	13.599(1)	13.606(2)	13.6036(7)	
V (Å³)	289.8(1)	290.12(7)	289.94(2)	
Z	6	6	6	
Grossular ($Ia\bar{3}d$)				
a (Å)	11.9650(5)	11.9673(7)		11.9435(2)
V (Å³)	1712.9(1)	1713.9(2)		1703.71(5)
Z	8	8		8
R_p (%)‖	3.58	3.88	3.59	3.73
R_{wp} (%)‖	4.82	5.55	4.86	5.04
R_e (%)‖	4.67	4.96	4.77	4.71
S‖	1.031	1.120	1.020	1.070
D-W d‖	1.120	0.968	1.208	1.051
Mass fraction#				
Cz	0.729	0.898	0.908	0.847
Esk	0.184	0.081	0.092	
Grs	0.087	0.021		0.153

* Step interval (°2θ) 10–130°, step 0.02°.
† Cr^{3+} in $Ca_2Al_{3-q}Cr_q^{3+}Si_3O_{12.5}$ gel-starting material.
‡ The Cr content refined without constraint was corrected by applying analytical line, $y = 1.364x - 0.004$, where x is Cr content (apfu) refined without constraint, and y is the corrected Cr content (apfu), and the analytical line was established based on the relationship between Cr contents determined by EPMA analyses and those refined by Rietveld analyses for epidotes in G27, G28, and G22 products.
§ Determined using EPMA.
‖ R_B = R-Bragg factor, R_F = R-structure factor, R_p = R-pattern, R_{wp}= R-weighted pattern, R_e = R-expected, S(=R_{wp}/R_e) = Goodness of fit (Young 1993), D-W d = Durbin-Watson d-statistic (Hill and Flack 1987).
Abbreviations as in Table 1.

and the number of step intervals, the estimated standard deviations (e.s.d.) for a Rietveld refinement can be made arbitrarily small (Scott 1983). The small e.s.d. values (1σ) in Table 4 may
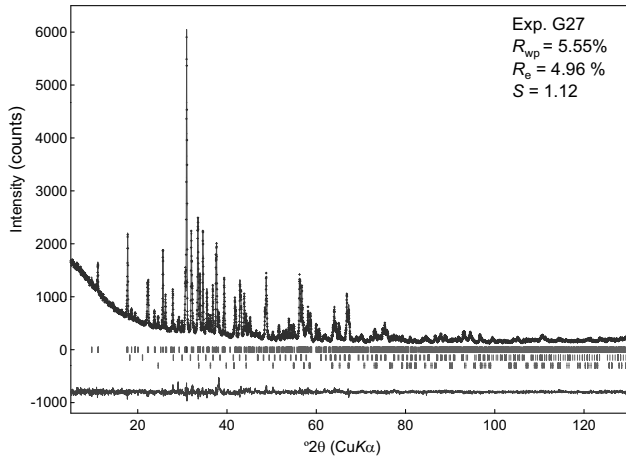
FIGURE 3. Rietveld refinement plot from experiment G27 consisting of Cr^{3+}-bearing clinozoisite, Cr-bearing grossular, and eskolaite. The crosses are the observed data, the solid line is the calculated pattern, and the vertical bars mark all possible Bragg reflections (for both $CuK\alpha_1$ and $K\alpha_2$). Upper, middle, and lower bars indicate the positions of reflections for Cr^{3+}-bearing clinozoisite, Cr-bearing grossular, and eskolaite, respectively. The difference in intensities between the observed and calculated pattern is show at the bottom.
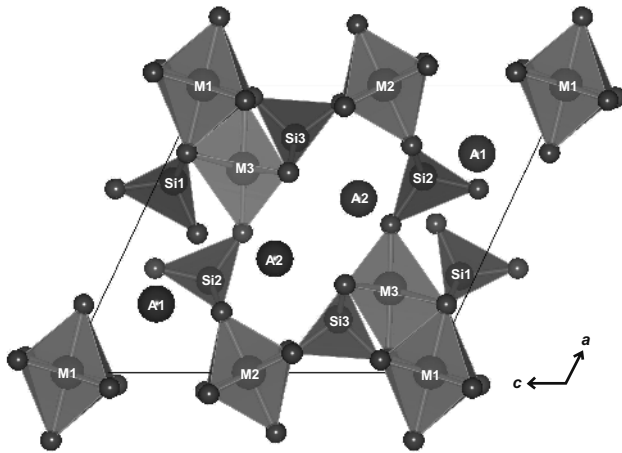

FIGURE 4. Crystal structure of clinozoisite from experiment G9 projected onto (010)—drafted using the program VESTA (Momma and Izumi 2008).

be a result of the long counting time that was 70–80 s/step. We give 3σ uncertainties for the cation occupancies at M1 and M3 (Table 5). However, because the B isotropic displacement parameters for the atoms were fixed in the refinement, the accuracy could be less.

DISCUSSION

Synthesis of Cr^{3+}-bearing clinozoisite

Clinozoisite was synthesized at P_{H_2O} = 0.8 to 1.5 GPa and T = 500 to 800 °C using gel-starting materials. The use of oxide starting materials resulted, instead, in the crystallization of quartz and chromatite ($CaCr^{6+}O_4$), which precluded crystallization of clinozoisite. We note that $Ca_2(Al,Mn^{3+})_3Si_3O_{12}(OH)$ piemontite

TABLE 4. Refined atomic positions

q^*		1.00	0.75		0.50
Site	x,y,z	G9	G27	G28	G22
T°C/P GPa		700/1.2	700/1.2	600/1.2	700/1.2
Cr^{3+} content (apfu)		0.62	0.50	0.49	0.28
O1	x	0.2358(9)	0.2390(8)	0.2336(7)	0.2350(9)
	y	0.992(2)	0.998(1)	0.995(1)	0.999(1)
	z	0.0432(8)	0.0459(7)	0.0432(6)	0.0421(7)
	B	0.70	0.70	0.70	0.70
O2	x	0.305(1)	0.3050(8)	0.3042(7)	0.2989(8)
	y	0.981(1)	0.980(1)	0.985(1)	0.986(1)
	z	0.349(1)	0.3514(9)	0.3535(7)	0.3485(9)
	B	0.63	0.63	0.63	0.63
O3	x	0.790(1)	0.7867(8)	0.7846(7)	0.7915(9)
	y	0.015(2)	0.010(1)	0.012(1)	0.019(1)
	z	0.3466(9)	0.3425(7)	0.3435(6)	0.3449(8)
	B	0.79	0.79	0.79	0.79
O4	x	0.054(1)	0.0569(9)	0.052(1)	0.051(1)
	y	1/4	1/4	1/4	1/4
	z	0.136(1)	0.138(1)	0.137(1)	0.134(1)
	B	0.6	0.6	0.6	0.6
O5	x	0.043(1)	0.041(1)	0.0423(9)	0.040(1)
	y	3/4	3/4	3/4	3/4
	z	0.153(1)	0.142(1)	0.145(1)	0.141(1)
	B	0.6	0.6	0.6	0.6
O6	x	0.066(1)	0.066(1)	0.062(1)	0.064(1)
	y	3/4	3/4	3/4	3/4
	z	0.405(1)	0.403(1)	0.401(1)	0.406(1)
	B	0.5	0.5	0.5	0.5
O7	x	0.518(1)	0.520(1)	0.520(1)	0.521(1)
	y	3/4	3/4	3/4	3/4
	z	0.177(1)	0.181(1)	0.1775(8)	0.179(1)
	B	0.6	0.6	0.6	0.6
O8	x	0.514(2)	0.515(1)	0.517(1)	0.512(2)
	y	1/4	1/4	1/4	1/4
	z	0.300(1)	0.299(1)	0.301(1)	0.297(1)
	B	0.9	0.9	0.9	0.9
O9	x	0.639(1)	0.636(1)	0.639(1)	0.641(1)
	y	1/4	1/4	1/4	1/4
	z	0.106(1)	0.107(1)	0.107(1)	0.109(1)
	B	1.0	1.0	1.0	1.0
O10	x	0.076(1)	0.073(1)	0.073(1)	0.076(1)
	y	1/4	1/4	1/4	1/4
	z	0.418(1)	0.417(1)	0.4187(9)	0.420(1)
	B	0.7	0.7	0.7	0.7
Ca1	x	0.7615(6)	0.7612(5)	0.7602(4)	0.7631(5)
	y	3/4	3/4	3/4	3/4
	z	0.1558(5)	0.1561(5)	0.1533(4)	0.1550(5)
	B	0.76	0.76	0.76	0.76
Ca2	x	0.6045(6)	0.6090(5)	0.6072(4)	0.6101(5)
	y	3/4	3/4	3/4	3/4
	z	0.4237(5)	0.4248(5)	0.4254(4)	0.4260(5)
	B	0.92	0.92	0.92	0.92
M1	x	0	0	0	0
	y	0	0	0	0
	z	0	0	0	0
	B	0.51	0.51	0.51	0.51
M2	x	0	0	0	0
	y	0	0	0	0
	z	1/2	1/2	1/2	1/2
	B	0.43	0.43	0.43	0.43
M3	x	0.2909(7)	0.2889(5)	0.2902(5)	0.2908(7)
	y	1/4	1/4	1/4	1/4
	z	0.2192(5)	0.2225(5)	0.2224(4)	0.2208(6)
	B	0.42	0.42	0.42	0.42
Si1	x	0.3346(7)	0.3392(6)	0.3374(5)	0.3359(6)
	y	3/4	3/4	3/4	3/4
	z	0.0440(7)	0.0463(6)	0.0486(5)	0.0478(6)
	B	0.41	0.41	0.41	0.41
Si2	x	0.6811(8)	0.6779(7)	0.6801(6)	0.6799(7)
	y	1/4	1/4	1/4	1/4
	z	0.2744(7)	0.2753(6)	0.2747(5)	0.2729(6)
	B	0.48	0.48	0.48	0.48
Si3	x	0.1847(8)	0.1816(6)	0.1833(6)	0.1801(7)
	y	3/4	3/4	3/4	3/4
	z	0.3225(8)	0.3191(6)	0.3187(5)	0.3164(7)
	B	0.42	0.42	0.42	0.42

Note: Estimated standard deviations are in parentheses (1σ).
* Cr^{3+} in $Ca_2Al_{3-q}Cr_q^{3+}Si_3O_{12.5}$ gel-starting material.

TABLE 5. Refined site occupancies at M1, M2, and M3

q^*	1.00	0.75		0.50
Synthesis P (GPa)	1.2	1.2	1.2	1.2
T (°C)	700	700	600	700
Exp. no.	G9	G27	G28	G22
Cr^{3+} content (apfu)	0.62	0.50	0.49	0.28
M1	Al0.75(1)Cr0.25(1)	Al0.78(1)Cr0.22(1)	Al0.79(1)Cr0.21(1)	Al0.88(1)Cr0.12(1)
M2	Al1.0	Al1.0	Al1.0	Al1.0
M3	Al0.63(1)Cr0.37(1)	Al0.72(1)Cr0.28(1)	Al0.72(1)Cr0.28(1)	Al0.84(1)Cr0.16(1)
K_D†	0.57	0.73	0.68	0.72

Note: Estimated standard deviations are in parentheses (3σ).
* Cr^{3+} in $Ca_2Al_{3-q}Cr^{3+}_qSi_3O_{12.5}$ gel-starting material.
† Distribution coeffient: $K_D = (Cr^{3+}/Al)^{M1}/(Cr^{3+}/Al)^{M3}$.

TABLE 6. Interatomic distances (Å)

q^*		1.00	0.75		0.50
Synthesis P (GPa)		1.2	1.2	1.2	1.2
T (°C)		700	700	600	700
Exp. no.		G9	G27	G28	G22
Cr^{3+} content (apfu)		0.62	0.50	0.49	0.28
Ca1-O1	×2	2.493(9)	2.488(7)	2.473(6)	2.450(8)
-O3	×2	2.367(9)	2.320(8)	2.360(7)	2.372(8)
-O5		2.52(1)	2.551(9)	2.543(8)	2.52(1)
-O6		2.81(1)	2.795(9)	2.783(8)	2.79(1)
-O7		2.27(1)	2.263(9)	2.250(8)	2.27(1)
Average		2.474	2.461	2.463	2.461
-O9	×2	2.971(4)	2.975(3)	2.965(3)	2.965(3)
Average		2.585	2.575	2.575	2.573
Ca2-O2	×2	2.760(8)	2.791(7)	2.799(8)	2.854(7)
-O2′	×2	2.58(1)	2.558(9)	2.519(7)	2.548(9)
-O3	×2	2.577(9)	2.538(7)	2.540(8)	2.583(8)
-O7		2.28(1)	2.25(1)	2.294(8)	2.28(1)
-O10		2.60(1)	2.59(1)	2.594(8)	2.55(1)
Average		2.589	2.577	2.576	2.600
-O8	×2	3.036(4)	3.043(4)	3.036(3)	3.054(4)
Average		2.679	2.670	2.668	2.691
Si1-O1	×2	1.614(9)	1.649(7)	1.641(6)	1.645(8)
-O7		1.61(1)	1.60(1)	1.590(8)	1.61(1)
-O9		1.64(1)	1.66(1)	1.68(1)	1.69(1)
Average		1.62	1.640	1.638	1.65
Si2-O3	×2	1.614(9)	1.626(7)	1.604(7)	1.603(8)
-O8		1.61(2)	1.57(1)	1.582(9)	1.61(1)
-O9		1.59(1)	1.59(1)	1.58(1)	1.55(1)
Average		1.61	1.60	1.593	1.59
Si3-O2	×2	1.627(7)	1.631(6)	1.639(6)	1.634(7)
-O5		1.64(1)	1.69(1)	1.670(9)	1.68(1)
-O6		1.60(1)	1.59(1)	1.62(1)	1.64(1)
Average		1.62	1.64	1.642	1.65
M1-O1	×2	1.950(7)	1.970(6)	1.929(6)	1.943(7)
-O4	×2	1.880(8)	1.890(7)	1.886(6)	1.867(7)
-O5	×2	2.004(9)	1.929(7)	1.948(6)	1.923(8)
Average		1.945	1.930	1.921	1.911
M2-O3	×2	1.853(8)	1.887(6)	1.895(6)	1.850(7)
-O6	×2	1.93(1)	1.942(9)	1.936(7)	1.909(9)
-O10	×2	1.896(8)	1.886(7)	1.876(6)	1.878(7)
Average		1.893	1.905	1.902	1.879
M3-O1	×2	2.185(8)	2.173(8)	2.195(7)	2.177(8)
-O2	×2	1.97(8)	1.964(8)	1.962(6)	1.946(8)
-O4		1.91(1)	1.86(1)	1.913(8)	1.92(1)
-O8		1.79(1)	1.82(1)	1.82(1)	1.78(1)
Average		2.002	1.992	2.008	1.991

Note: Estimated standard deviations are in parentheses (1σ).
* Cr^{3+} in $Ca_2Al_{3-q}Cr^{3+}_qSi_3O_{12.5}$ gel-starting material.

TABLE 7. Selected interatomic angles (°)

q^*	1.00	0.75		0.50
Synthesis P (GPa)	1.2	1.2	1.2	1.2
T (°C)	700	700	600	700
Exp. no.	G9	G27	G28	G22
Cr^{3+} content (apfu)	0.62	0.50	0.49	0.28
O1-Si1-O1′	114.4(7)	114.8(6)	113.5(5)	115.9(6)
O1-Si1-O7	110.9(4)	110.2(4)	112.9(3)	112.1(4)
O1-Si1-O9	106.8(4)	106.6(3)	105.2(3)	104.5(3)
O7-Si1-O9	106.5(6)	108.2(6)	106.2(5)	106.6(6)
O3-Si2-O3′	109.5(7)	111.6(6)	112.5(5)	107.6(6)
O3-Si2-O8	110.0(5)	111.0(4)	109.1(3)	111.3(4)
O3-Si2-O9	108.0(5)	106.0(4)	107.0(3)	107.5(4)
O8-Si2-O9	111.3(8)	111.0(7)	112.0(5)	111.6(7)
O2-Si3-O2′	105.5(7)	104.3(5)	106.9(5)	107.9(6)
O2-Si3-O5	109.2(5)	109.9(4)	110.7(3)	109.5(4)
O2-Si3-O6	116.5(4)	115.1(4)	114.1(3)	113.2(4)
O5-Si3-O6	99.6(6)	102.5(5)	100.4(5)	103.3(6)
O1-M1-O4	86.5(4)	84.8(3)	86.7(3)	86.5(4)
O1-M1-O5	91.2(4)	91.2(3)	91.3(3)	90.3(3)
O4-M1-O5	92.7(3)	94.5(3)	94.0(3)	95.4(3)
O3-M2-O6	91.4(4)	90.2(3)	90.0(3)	91.2(4)
O3-M2-O10	89.0(4)	89.3(3)	88.8(3)	89.8(4)
O6-M2-O10	94.4(3)	94.2(3)	94.8(3)	95.2(3)
O1-M3-O1′	82.9(4)	81.0(4)	81.2(3)	80.4(4)
O1-M3-O2	88.2(3)	88.9(3)	89.7(2)	89.7(3)
O1-M3-O4	79.5(3)	79.9(3)	78.9(2)	78.8(3)
O1-M3-O8	101.1(3)	98.7(3)	100.4(3)	100.3(3)
O2-M3-O2′	99.8(5)	100.7(4)	98.4(4)	98.8(4)
O2-M3-O4	92.2(3)	93.3(3)	92.5(2)	91.3(3)
O2-M3-O8	87.3(3)	87.9(3)	88.0(2)	89.5(3)
Si1-O9-Si2	160.2(8)	160.9(7)	161.5(6)	162.1(8)

Note: Estimated standard deviations are in parentheses (1σ).
* $q = Cr^{3+}$ in $Ca_2Al_{3-q}Cr^{3+}_qSi_3O_{12.5}$ gel-starting material.

(2006), who found that it can be obtained at pressures less than 0.50 GPa using $CaFe^{3+}AlSiO_6$ pyroxene instead of hematite as a Fe^{3+}-containing starting material. For the study here, the gel-starting materials played an important role in allowing the crystallization of Cr^{3+}-bearing clinozoisite.

The role of the fluid phase has been emphasized in the formation of Cr-containing metamorphic minerals (e.g., Treloar 1987). It transports Cr^{3+} that is set free by the breakdown of chromite and chemically modifies various silicates such as epidote, muscovite, amphibole, and pyroxene (Treloar 1987; Sánchez-Vizcaíno et al. 1995; Nagashima et al. 2006), pumpellyite (Mevel and Kienast 1980; Enami 1986; Hamada et al. 2008), and sodic pyroxene, phengite, and allanite (Banno 1993). Such natural processes for the formation of Cr-rich metamorphic minerals indicates that a synmetamorphic fluid responsible for the alteration of detrital chromite precipitated chromian silicates or resulted in Cr-enrichment of Cr-poor minerals (Challis et al. 1995). The fact that Cr^{3+} contents of clinozoisite, associated with small amounts of eskolaite, were less than those in the starting

was synthesized from oxide starting materials at low pressures of 0.20–0.35 GPa (Strens 1964; Keskinen and Liou 1979; Nagashima and Akasaka 2004), but pressures greater than 0.50 GPa are required for the crystallization of $Ca_2(Al,Fe^{3+})_3Si_3O_{12}(OH)$ epidote from oxide starting materials. Here, hematite crystallizes at pressures less than 0.50 GPa and it interferes with the crystallization of epidote (Liou 1973; Nagashima 2006). The difficulty in crystallizing Al-Fe^{3+} epidote was overcome by Nagashima

materials (Table 2) indicates that the present experiments show an opposite process: Cr^{3+} was distributed homogeneously in the gel-starting material and in the crystallization process of oxide and silicate, Cr^{3+} was more concentrated into the oxide (eskolaite in this experiment).

Cr^{3+}-bearing clinozoisite and zoisite crystallized from the Cr-poor starting gel with $q = 0.25$. Crystallization of both clinozoisite and zoisite together was reported for Al-rich compositions along the $Ca_2Al_3Si_3O_{12}(OH)$-$Ca_2Al_2Fe^{3+}Si_3O_{12}(OH)$ join (Prunier and Hewitt 1985; Brunsmann et al. 2002) and for the $Ca_2Al_3Si_3O_{12}(OH)$-$Ca_2Mn_3^{3+}Si_3O_{12}(OH)$ join (Anastasiou and Langer 1977; Langer et al. 2002). Thus, this result is consistent with other synthesis studies of epidote-group minerals. Brunsmann et al. (2002) showed that zoisite contained no more than 0.11 Fe^{3+} apfu at 0.5 GPa and 650 °C and ca. 0.16 Fe^{3+} at 2.0 GPa and 800 °C. In the present study, zoisite synthesized at 1.2 GPa and 600 and 700 °C contained a maximum of 0.19 apfu Cr^{3+}. One possible explanation for the greater Cr^{3+} contents, compared to Fe^{3+}, may be related to the slightly smaller ionic radius of Cr^{3+} (0.62 Å; Shannon 1976) compared to that of Fe^{3+} (0.645 Å).

Chromium occupancies at the octahedral sites

In epidote-group minerals, the M3 octahedron is larger and more distorted than M1 and M2 (Ito et al. 1954; Dollase 1968). The volumes of the three crystallographically independent octahedra decrease as M3 > M1 > M2. M2 is the least distorted octahedron. The different octahedral volumes affect the partitioning behavior of transition elements over the three sites. For clinozoisite from Outokumpu, Finland, with ca. 1 Cr^{3+} apfu, Treloar (1987) proposed that Cr^{3+} is preferentially partitioned into M1. This proposal was based on the early optical absorption spectroscopic study of Burns and Strens (1967), who concluded that Cr^{3+} had a strong preference for M1. However, Liebscher (2004) questioned their assignment because it would give rise to a Racah parameter that is larger than that of a free Cr^{3+} ion and therefore made no physical sense.

Our refinement results indicate that Cr^{3+} has a greater preference for M3 than for M1 (Fig. 5). This agrees with the Cr^{3+} partitioning behavior observed in natural epidote (Nagashima et al. 2007; Armbruster et al. 2006). The distribution coefficient K_D = $(Cr^{3+}/Al)^{M1}/(Cr^{3+}/Al)^{M3}$ for the Iratsu epidote has values from 0.35 to 0.41, whereas the K_D values for synthetic clinozoisite are larger, having values between 0.59 and 0.73 (Fig. 6). At present, the reason for the differences in the K_D values between the Iratsu epidote and the present synthetic clinozoisite is not clear, and more study under systematically controlled P, T, and X conditions may give a solution. The Cr-Al K_D values are significantly larger than those associated with Fe^{3+}-Al partitioning, where K_D = $(Fe^{3+}/Al)^{M1}/(Fe^{3+}/Al)^{M3}$ = 0.033–0.054 for epidote synthesized at 0.46–0.55 GPa and 700 °C (Giuli et al. 1999) and also for Mn^{3+}-Al partitioning, where K_D values [$(Mn^{3+}/Al)^{M1}/(Mn^{3+}/Al)^{M3}$] for piemontite synthesized at 1.5 GPa and 800 °C (Langer et al. 2002) and at 0.20–0.35 GPa and 500 °C (Nagashima and Akasaka 2004) are 0.063–0.080 and 0.038–0.063, respectively. The preference of Cr^{3+} for M1 is stronger than that of Fe^{3+} and Mn^{3+}, which might be related to the smaller ionic radius of Cr^{3+} compared to those of Fe^{3+} or Mn^{3+} (0.645 Å).
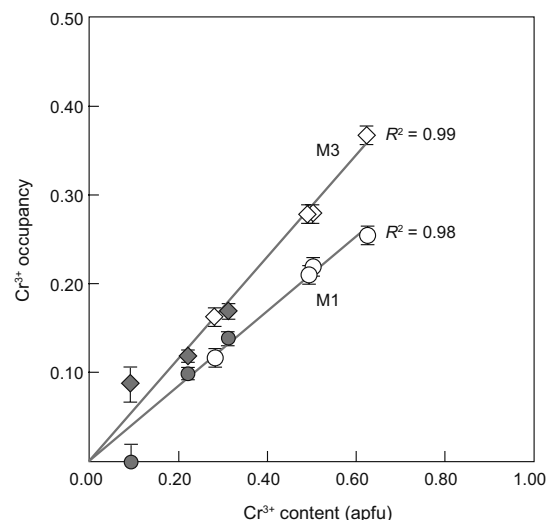

FIGURE 5. Variation in Cr^{3+} occupancy at M1 and M3 as a function of total Cr^{3+} content in clinozoisite and epidote. Open symbols represent Cr^{3+}-bearing clinozoisite (this study), gray symbols natural Iratsu epidote (Nagashima et al. 2007), and the diamonds represent the Cr^{3+} occupancy at M3 and the circles at M1. Error bars represent 3σ standard deviations.
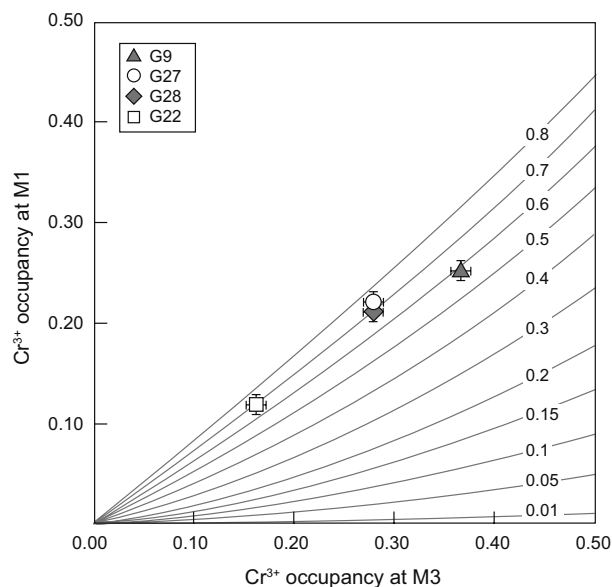

FIGURE 6. Cr^{3+} occupancy at M1 vs. Cr^{3+} occupancy at M3. Numbered lines indicate $K_D = (Cr^{3+}/Al)^{M1}/(Cr^{3+}/Al)^{M3}$.

Unit-cell parameters and bond lengths

Variations in unit-cell parameters were observed as a function of Cr^{3+} contents at M1 and M3 in natural epidote (Nagashima et al. 2007). However, the Iratsu epidote contains a small amount of Sr and moderate amounts of Fe^{3+}. Thus, its unit-cell parameters are also affected by the exchange of Fe^{3+} for Al and Sr for Ca. The results of this work allow an analysis of unit-cell parameters for strictly binary $Ca_2Al_3Si_3O_{12}(OH)$-$Ca_2Al_2CrSi_3O_{12}(OH)$ solid solutions (Fig. 7). Unit-cell parameters for clinozoisite of composition $[Ca_{1.00}]^{A1}[Ca_{1.00}]^{A2}[Al_{1.00}]^{M1}[Al_{1.00}]^{M2}[Al_{0.96}Fe_{0.04}]^{M3}Si_3O_{12}(OH)$ from Dollase (1968) and for synthetic epidote on

the $Ca_2Al_3Si_3O_{12}(OH)$-$Ca_2Al_2Fe^{3+}Si_3O_{12}(OH)$ join (Giuli et al. 1999) are also shown. Unit-cell parameters for Al-Cr^{3+} clinozoisite and Al-Fe^{3+} epidote increase linearly with increasing Cr^{3+} and Fe^{3+} contents, respectively. However, variations in a, b, c, and V for clinozoisite are smaller than those for epidote. It is also observed that the β angles for synthetic Cr-bearing clinozoisite are smaller than those for natural Cr-free clinozoisite (Dollase 1968) and synthetic epidote (Giuli et al. 1999). Unit-cell behavior appears somewhat different than the non-linear variations associated with Mn^{3+} substitution in Al-Mn^{3+} piemontite (Anastasiou and Langer 1977; Langer et al. 2002; Nagashima and Akasaka 2004).

Mean M1-O and M3-O distances, given as <M1-O> and <M3-O>, increase with increasing Cr at M1 and M3. We selected quadratic fits to data for Cr^{3+}-bearing clinozoisite to link them to the corresponding sites in Dollase's (1968) Fe-poor natural clinozoisite; the <M1-O> and <M3-O> distances in this clinozoisite should, in principle, be the shortest in the $Ca_2Al_3Si_3O_{12}(OH)$-$Ca_2Al_2Cr^{3+}Si_3O_{12}(OH)$ series. The <M1-O> and <M3-O> varia-

tions (Fig. 8) can be described by the relationships:

$$<M1-O> = 1.014x^2 - 0.121x + 1.907 \ (R^2 = 0.93),$$

and

$$<M3-O> = -0.186x^2 + 0.148x + 1.973 \ (R^2 = 0.73),$$

where x is the Cr content (apfu) at M1 or M3.

Variations in <M1-O> are greater than those for <M3-O>. <M1-O> distances for the Iratsu Cr^{3+}-bearing epidote plot on the <M1-O> trend defined by the synthetic Cr^{3+}-bearing clinozoisite, whereas its <M3-O> distances are longer. This is consistent with Cr^{3+} alone substituting for Al at M1 and with 0.48–0.51 apfu Fe^{3+} as well as Cr^{3+} substituting for Al at M3 in the Iratsu Cr^{3+}-bearing epidote (Nagashima et al. 2007). In $Ca_2(Al,Fe^{3+},Mn^{3+})_3Si_3O_{12}(OH)$ epidote-group minerals, variations in unit-cell parameters are mainly caused by volume changes associated with the $M3O_6$ octahedra (Nagashima and Akasaka 2004), because Fe^{3+} and Mn^{3+} ions strongly prefer M3 over M1. On the other hand, in Cr^{3+}-bearing clinozoisite the increase in unit-cell parameters is caused by an increase in volume of both $M3O_6$ and $M1O_6$ octahedra, where both contain Cr.

Variations in M3-O1, M3-O2, M3-O4, and M3-O8 distances for the Iratsu epidote as a function of the mean ionic radius (r, Å) of the M cations are similar in behavior (Nagashima et al. 2007) (Fig. 9a). This indicates an equidimensional expansion of the $M3O_6$ octahedra with the substitution of Cr^{3+} (+Fe^{3+}) for Al^{3+}. <M3-O> distances as a function of mean ionic radius, derived from the data of Nagashima et al. (2007) and those in this study, are given by:

$$<M3-O> \ (\text{Å}) = 0.466r + 1.734 \ (R^2 = 0.73).$$

FIGURE 7. Variation in unit-cell parameters as a function of Cr^{3+} or Fe^{3+} contents in clinozoisite and epidote. Open diamonds represent synthetic Cr^{3+}-bearing clinozoisite (this study), the filled triangle a natural clinozoisite with 0.03 Fe^{3+} at M3 (Dollase 1968), and the filled squares synthetic epidote (Giuli et al. 1999). Error bars represent 1σ standard deviation. Some symbols lack error bars because symbols are larger than error bars.
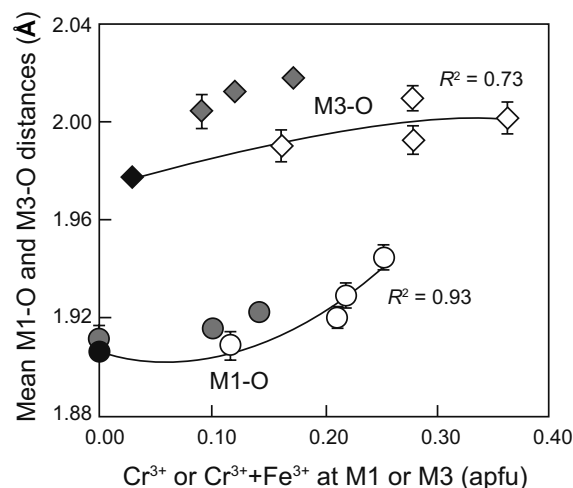

FIGURE 8. Variations in mean M1-O and M3-O distances as a function of Cr^{3+} or Cr^{3+}+Fe^{3+} content at the M1 and M3 sites. Open symbols represent synthetic Cr^{3+}-bearing clinozoisite (this study), gray symbols natural Iratsu epidote (Nagashima et al. 2007), filled symbols natural clinozoisite (Dollase 1968), the diamonds represent mean M3-O, and the circles mean M1-O values. Error bars represent 1σ standard deviation. Some symbols lack error bars because symbols are larger than error bars.
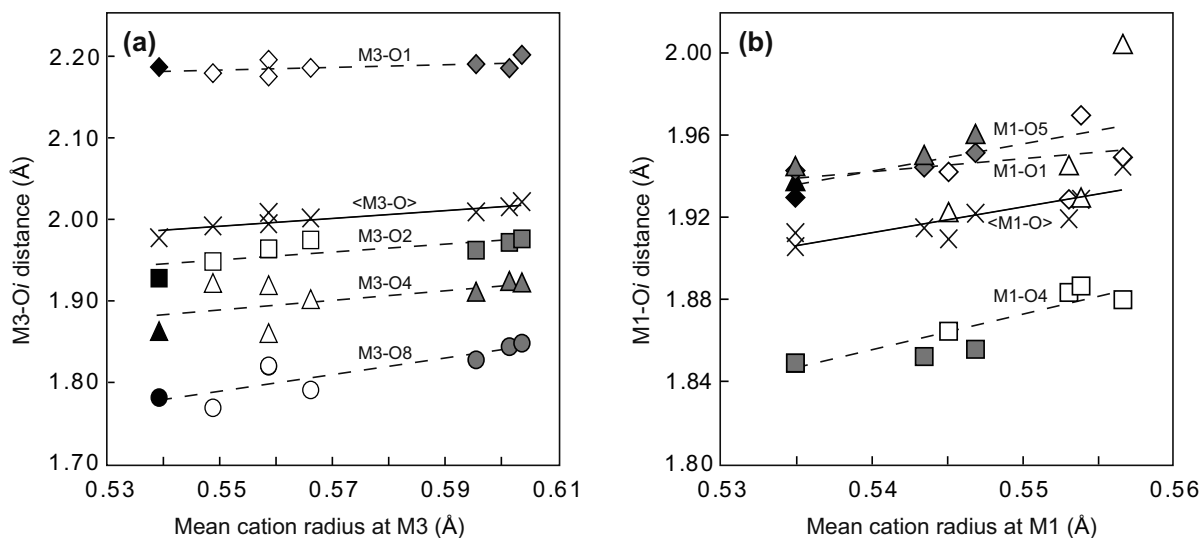
FIGURE 9. (**a**) M3-Oi distances and (**b**) M1-Oi distances for Cr^{3+}-bearing clinozoisite and epidote, respectively, as a function of the mean cation radius at the M3 and M1. (**a**) Open symbols represent synthetic Cr^{3+}-bearing clinozoisite (this study), the gray symbols natural Iratsu epidote (Nagashima et al. 2007), and the filled symbols a natural clinozoisite (Dollase 1968). The diamonds represent the M3-O1 distances, the squares M3-O2, the triangles M3-O4, the circles M3-O8, and the crosses <M3-O>. (**b**) Open symbols represent synthetic Cr^{3+}-bearing clinozoisite (this study), gray symbols Iratsu epidote (Nagashima et al. 2007), filled symbols natural clinozoisite (Dollase 1968), diamonds M1-O1, squares M1-O4, triangles M1-O5, and crosses <M1-O>.

They reported similar variations for M1-O1, M1-O4, and M1-O5 distances with increasing Cr^{3+} content at M1. The M1-O1 and M1-O5 lengths from this study are somewhat variable, but similar (Fig. 9b). The <M1-O> distance is related to the mean ionic radius of the central cation radius of the M1 cation through:

$$<M1-O> = 1.304r + 1.202 \ (R^2 = 0.66).$$

Although <M1-O> is shorter than <M3-O>, the increase in <M1-O> with mean ionic radius is 2.8 times greater. This is consistent with the distribution of Cr^{3+} between M1 and M3 and the larger volume of M3O$_6$ compared to M1O$_6$.

ACKNOWLEDGMENTS

REFERENCES CITED

Akasaka, M., Zheng, Y., and Suzuki, Y. (2000) Maximum strontium content of piemontite formed by hydrothermal synthesis. Journal of Mineralogical and Petrological Sciences, 95, 84–94.
Anastasiou, P. and Langer, K. (1977) Synthesis and physical properties of piemontite Ca$_2$Al$_{3-p}$Mn$_p^{3+}$(Si$_2$O$_7$/SiO$_4$/O/OH). Contributions to Mineralogy and Petrology, 60, 225–245.
Armbruster, T., Bonazzi, P., Akasaka, M., Bermanec, V., Chopin, C., Heuss-

Assbischler, S., Liebscher, A., Menchetti, S., Pan, Y., and Pasero, M. (2006) Recommended nomenclature of epidote-group minerals. European Journal of Mineralogy, 18, 551–567.
Ashley, P.M. and Martyn, J.E. (1987) Chromium-bearing minerals from a meta-morphosed hydrothermal alteration zone in the Archean of Western Australia. Neues Jahrbuch für Mineralogie Abhandlungen, 157, 81–111.
Banno, Y. (1993) Chromian sodic pyroxene, phengite and allanite from the San-bagawa blueschists in the eastern Kii Peninsula, central Japan. Mineralogical Journal, 16, 306–317.
Bastin, G.F., van Loo, F.J.J., and Heijlingers, H.J.M. (1984) Evaluation of the use of Gaussian φ(ρz) curves in quantitative electron probe microanalysis: A new optimization. X-ray Spectrometry, 13, 91–97.
Bastin, G.F., Heijlingers, H.J.M., and van Loo, F.J.J. (1986) A further improvement in the Gaussian φ(ρz) approach for matrix correction in quantitative electron probe microanalysis. Scanning, 8, 45–67.
Bish, D.L. and Reynolds, R.C. (1989) Sample preparation for X-ray diffraction. In D.L. Bish and J.E. Post, Eds., Modern Powder Diffraction, 20, p. 73–99. Reviews in Mineralogy, Mineralogical Society of America, Chantilly, Virginia.
Bleeck, A.W.G. (1907) Die Jadeitlagerstätten in Upper Burma. Zeitschrift für Praktische Geologie, 341–365.
Brunsmann, A., Franz, G., and Heinrich, W. (2002) Experimental investigation of zoisite-clinozoisite phase equilibria in the system CaO-Fe$_2$O$_3$-Al$_2$O$_3$-SiO$_2$-H$_2$O. Contributions to Mineralogy and Petrology, 143, 115–130.
Burns, R.G. and Strens, R.G.J. (1967) Structural interpretation of polarized absorption spectra of the Al-Fe-Mn-Cr epidotes. Mineralogical Magazine, 36, 204–226.
Cemic, L., Geiger, C.A., Hoyer, W., Koch-Müller, M., and Langer, K. (1990) Piston-cylinder techniques: Pressure and temperature calibration of a pyrophyl-lite-based assembly by means of DTA measurements, a salt-based assembly, and a cold-sealing encapsulation method. Neues Jahrbuch für Mineralogie Monatshefte, H.2, 49–64.
Challis, A., Grapes, R., and Palmer, K. (1995) Chromian muscovite, uvarovite, and zincian chromite: Products of regional metasomatism in northwest Nelson, New Zealan. Canadian Mineralogist, 33, 1263–1284.
Coes Jr., L. (1955) High pressure minerals. Journal of American Ceramic Society, 38, 298.
Deer, W.A., Howie, R.A., and Zussman, J. (1986) Rock-Forming Minerals, Vol. 1B: Disilicates and Ring Silicates, 629 p. Geological Society Publishing House, Bath, U.K.
Devaraju, T.C., Raith, M.M., and Spiering, B. (1999) Mineralogy of the Archean barite deposit of Ghattihosahalli, Karnataka India. Canadian Mineralogist, 37, 603–617.
Dollase, W.A. (1968) Refinement and comparison of the structures of zoisite and clinozoisite. American Mineralogist, 53, 1882–1898.
——— (1971) Refinement of the crystal structures of epidote, allanite, and han-

cockite. American Mineralogist, 56, 447–464.
——— (1986) Correction of intensities for preferred orientation in powder diffractometry: application of the March model. Journal of Applied Crystallography, 19, 267–272.

Enami, M. (1986) Chromian and titanian pumpellyites in a metagabbro pebble from the Miocene sediments in the Chita Peninsula, central Japan. Mineralogical Journal, 13, 90–97.

Eskola, P. (1920) The mineral facies of rocks. Norsk Geologisk Tidsskrift, 6, 143–194.
——— (1933) On the chrome minerals of Outokumpu. Bulletin de la Commission Géologique de Finlande, 103, 26–44.

Fyfe, W.S. (1960) Stability of epidote minerals. Nature, 187, 497–498.

Geiger, C.A. and Armbruster, T. (1997) $Mn_3Al_2Si_3O_{12}$ spessartine and $Ca_3Al_2Si_3O_{12}$ grossular garnet: Structural dynamic and thermodynamic properties. American Mineralogist, 82, 740–747.

Giuli, G., Bonazzi, P., and Menchetti, S. (1999) Al-Fe disorder in synthetic epidotes: A single-crystal X-ray diffraction study. American Mineralogist, 84, 933–936.

Grapes, R.H. (1981) Chromian epidote and zoisite in kyanite amphibolites, Southern Alps, New Zealand. American Mineralogist, 66, 974–975.

Hamada, M., Seto, S., Akasaka, M., and Takasu, A. (2008) Chromian pumpellyite and associated chromian minerals from Sangun metamorphic rocks, Osayama, southwest Japan. Journal of Mineralogical and Petrological Sciences, 103, 390–399.

Hamilton, D.L. and Henderson, C.M.B. (1968) The preparation of silicate compositions by a gelling method. Mineralogical Magazine, 36, 832–838.

Hill, R.J. and Flack, H.D. (1987) The use of the Durbin-Watson d statistic in Rietveld analysis. Journal of Applied Crystallography, 20, 356–361.

Hill, R.J. and Madsen, I.C. (1986) The effect of profile step width on the determination of crystal structure parameters and estimated standard deviations by X-ray Rietveld analysis. Journal of Applied Crystallography, 19, 10–18.

Holdaway, M.J. (1966) Hydrothermal stability of clinozoisite plus quartz. American Journal of Science, 264, 643–667.
——— (1972) Thermal stability of Al-Fe epidote as a function of f_{O_2} and Fe content. Contributions to Mineralogy and Petrology, 37, 307–340.

Ito, T., Morimoto, N., and Sadanaga, R. (1954) On the structure of epidote. Acta Crystallographica, 7, 53–59.

Izumi, F. (1993) Rietveld analysis program RIETAN and PREMOS and special applications. In R.A. Young, Ed., The Rietveld Method, p. 236–253. Oxford Science Publications, U.K.

Izumi, F. and Ikeda, T. (2000) A Rietveld analysis program RIETAN-98 and its application to zeolites. Material Science Forum, 321–324.

Izumi, F. and Momma, K. (2007) Three-dimensional visualization in powder diffraction. Solid State Phenomena, 130, 15–20.

Keskinen, M. and Liou, J.G. (1979) Synthesis and stability relations of Mn-Al piemontite, $Ca_2MnAl_2Si_3O_{12}(OH)$. American Mineralogist, 64, 317–328.
——— (1987) Stability relations of Mn-Fe-Al piemontite. Journal of Metamorphic Geology, 5, 495–507.

Langer, K., Tillmanns, E., Kersten, M., Almen, H., and Arni, R.K. (2002) The crystal chemistry of Mn^{3+} in the clino- and orthozoisite structure types, $Ca_2M_3^{3+}$ $[OH/O/SiO_4/Si_2O_7]$: A structural and spectroscopic study of some natural piemontites and "thulites" and their synthetic equivalents. Zeitschrift für Kristallographie, 217, 1–18.

Liebscher, A. (2004) Spectroscopy of epidote minerals. In A. Liebscher and G. Franz, Eds., Epidotes, 56, p. 125–170. Reviews in Mineralogy and Geochemistry, Mineralogical Society of America, Chantilly, Virginia.

Liou, J.G. (1973) Synthesis and stability relations of epidote, $Ca_2Al_2FeSi_3O_{12}(OH)$. Journal of Petrology, 14, 381–413.

Mevel, C. and Kienast, J.R. (1980) Chromian jadeite, phengite, pumpellyite, and lawsonite in a high-pressure metamorphosed gabbro from the French Alps. Mineralogical Magazine, 43, 979–984.

Momma, K. and Izumi, F. (2008) VESTA: a three-dimensional visualization system for electronic and structural analysis. Journal of Applied Crystallography, 41, 653–658.

Nagashima, M. (2006) Hydrothermal syntheses of epidote and piemontites on the join $Ca_2Al_2Fe^{3+}Si_3O_{12}(OH)$-$Ca_2Al_2Mn^{3+}Si_3O_{12}(OH)$ at relatively low pressures of 200–400 MPa. Journal of Mineralogical and Petrological Sciences, 101, 1–9.

Nagashima, M. and Akasaka, M. (2004) An X-ray Rietveld study of piemontite on the join $Ca_2Al_3Si_3O_{12}(OH)$-$Ca_2Mn_3^{3+}Si_3O_{12}(OH)$ formed by hydrothermal synthesis. American Mineralogist, 89, 1119–1129.

Nagashima, M., Akasaka, M., and Sakurai, T. (2006) Chromian epidote in omphacite rocks from the Sambagawa metamorphic belt, central Shikoku, Japan. Journal of Mineralogical and Petrological Sciences, 101, 157–169.

Nagashima, M., Akasaka, M., Kyono, A., Makino, K., and Ikeda, K. (2007) Distribution of chromium among the octahedral sites in chromian epidote from Iratsu, central Shikoku, Japan. Journal of Mineralogical and Petrological Sciences, 102, 240–254.

Newnham, R.E. and De Haan, Y.M. (1962) Refinement of the α-Al_2O_3, Ti_2O_3, V_2O_3, and Cr_2O_3 structures. Zeitschrift Kristallographie, 117, 235–257.

Packwood, R.H. and Brown J.D. (1981) A Gaussian expression to describe $\phi(\rho z)$ curves for quantitative electron probe microanalysis. X-ray Spectrometry, 10, 138–146.

Post, J.E. and Bish, D.L. (1989) Rietveld refinement of crystal structures using powder X-ray diffraction data. In D.L. Bish and J.E. Post, Eds., Modern Powder Diffraction, 20, p. 277–308. Reviews in Mineralogy, Mineralogical Society of America, Chantilly, Virginia.

Prunier, A.R. and Hewitt, D.A. (1985) Experimental observations on coexisting zoisite-clinozoisite. American Mineralogist, 70, 375–378.

Rietveld, H.M. (1967) Line profiles of neutron powder-diffraction peaks for structure refinement. Acta Crystallographica, 22, 151–152.

Sánchez-Vizcaíno, V.L., Franz, G., and Gómez-Pugnaire, M.T. (1995) The behavior of Cr during metamorphism of carbonate rocks from the Nevado-Filabride complex, Betic Cordilleras, Spain. Canadian Mineralogist, 33, 85–104.

Schiffman, P. and Liou, J.G. (1983) Synthesis of Fe-pumpellyite and its stability relations with epidote. Journal of Metamorphic Geology, 1, 91–101.

Scott, H.G. (1983) The estimation of standard deviations in powder diffraction Rietveld refinements. Journal of Applied Crystallography, 16, 159–163.

Shannon, R.D. (1976) Revised effective ionic radii and systematic studies of interatomic distances in halides and chalcogenides. Acta Crystallographica, A32, 751–767.

Strens, R.G.J. (1964) Synthesis and properties of piemontite. Nature, 201, 175–176.

Toraya, H. (1990) Array-type universal profile function for powder pattern fitting. Journal of Applied Crystallography, 23, 485–491.

Treloar, P. (1987) The Cr-minerals of Outokumpu—Their chemistry and significance. Journal of Petrology, 28, 867–886.

Winkler, H.G.F. and Nitsch, N.H. (1963) Bildung von Epidot. Naturwissenschaften, 50, 612–613.

Young, R.A. (1993) Introduction to the Rietveld method. In R.A. Young, Ed., The Rietveld Method, p. 1–38. Oxford Science Publications, U.K.